Steinberger, B., Conrad, C. P., Osei Tutu, A., Hoggard, M. J. (2019): On the amplitude of dynamic topography at spherical harmonic degree two. - *Tectonophysics*, *760*, 5, pp. 221—228.

DOI: http://doi.org/10.1016/j.tecto.2017.11.032

On the amplitude of dynamic topography at spherical harmonic degree two

Bernhard Steinberger[a,b,*], Clinton P. Conrad[b], Anthony Osei Tutu[a], Mark J. Hoggard[c]

[a] *GFZ German Research Centre for Geosciences, Telegrafenberg, 14473 Potsdam, Germany*
[b] *Centre for Earth Evolution and Dynamics, University of Oslo, PO Box 1028, 0315 Oslo, Norway*
[c] *Bullard Laboratories, University of Cambridge, Madingley Road, Cambridge, CB3 0EZ, UK*

Abstract

Two large, seismically slow regions in the lower mantle beneath Africa and the Pacific Ocean are sometimes referred to as "superplumes". This name evokes images of large-scale active upwellings. However, it remains unclear whether these features are real or represent collections of multiple regular mantle plumes. Here, we investigate the implications of these upwellings for dynamic topography. We combine detailed measurements of oceanic residual topography from Hoggard et al. (2016) with continental constraints derived from CRUST1.0 to produce a global model expanded in spherical harmonics. Observed dynamic topography is subsequently compared to predictions derived from mantle flow following Steinberger (2016) using tomographic density models. Results yield relatively good overall agreement and amplitude spectra with similar slopes, except for degree two (i.e. $> 10,000$ km wavelengths) where predicted amplitude is more than two times as large and is dominated by contributions from the lower mantle. Predictive models suggest two large-scale uplifted regions above the "superplumes" that are barely seen in the observed topography. We suggest that this mismatch can only partly be reconciled by altering the seismic velocity to density conversion factor or by including the effects of lower mantle chemical heterogeneity. In addition, it may be important to consider more significiant revisions to the lower mantle flow patterns, such as those possibly induced by different radial viscosity profiles and laterally-varying or anisotropic lower mantle viscosity.

Keywords: dynamic topography, large-scale mantle structure, seismic tomography, mantle viscosity, mantle convection, superplumes

1. Introduction

Earth's Large Low Shear Velocity Provinces (LLSVPs) are prominent and robust lower mantle features that are consistently recovered in seismic tomography models (Dziewonski et al., 1977; Su and Dziewonski, 1991; Lekic et al., 2012). Located beneath Africa and the Pacific Ocean, these approximately antipodal structures correspond to a prominent spherical harmonic degree two signal. They extend for several thousand km laterally and probably several hundred km radially above the core-mantle boundary on average, in some places perhaps even 1000-1500 km. Within them, shear velocities are reduced by more than 1 % below average. Initially, these features were thought to represent purely thermal upwellings (e.g. Figure 4 of Courtillot et al., 2003), which has led to them sometimes being referred to as "superplumes" (Dziewonski et al., 2010). Although still debated, an alternative view has emerged that the LLSVPs are chemically distinct piles that may be denser than surrounding and overlying mantle and remain stable in the lowermost mantle as a result (Garnero et al., 2016). Supporting evidence for this viewpoint comes from seismology,

*Corresponding author; e-mail: bstein@gfz-potsdam.de, phone: +49-331-288-1881

with the anti-correlation of s-wave and bulk sound anomalies complementing requirements for excess density from normal mode tomography (Su and Dziewonski, 1997; Masters et al., 2000; Ishii and Tromp, 2004) and analysis of whole-Earth body tides independently providing evidence for increased density (Lau et al., 2017). A chemical heterogeneity is also suggested by strong horizontal velocity gradients, often in excess of 0.2 % per degree of arc near their edges, around the -1 % contour (Torsvik et al., 2006). Localized seismological studies also show that LLSVPs have steep edges with strong horizontal gradients (e.g. Masters et al., 2000; Ni et al., 2002; Wang and Wen, 2004; To et al., 2005; Frost and Rost, 2014). Such interfaces may localize upwellings arising from the core-mantle boundary (Steinberger and Torsvik, 2012), and indeed hotspot volcanism is found to occur preferentially above the LLSVP margins (Thorne et al., 2004). A cartoon cross section from this viewpoint is shown in Figure 5c of the paper by Torsvik in this issue – originally from Torsvik et al. (2016). A review of LLSVPs is given by McNamara in this issue.

It is important to note that the dynamics of the LLSVPs are still debated. For example, some authors have proposed that the LLSVPs may be clusters of poorly-resolved individual plumes (Lassak et al., 2010) or part of larger layered thermochemical structures extending through the lower mantle (Ballmer et al., 2016). Some seismological studies have questioned a thermochemical explanation by suggesting that lower mantle heterogeneity is best explained by thermal variations (Davies et al., 2012; Schuberth et al., 2012; Koelemeijer et al., 2017). Other studies have used statistical analysis to interrogate the correlation between LLSVP margin locations and volcanism (Austermann et al., 2014; Davies et al., 2015; Doubrovine et al., 2016). Geodynamic models have been used to examine the stability of the LLSVPs within the expected background mantle flow field (Bull et al., 2014). Indeed, these questions relating to the nature and stability of LLSVPs have been a recurring theme in the work of Trond Torsvik, to whom this volume is dedicated (e.g. Torsvik et al., 2006, 2016). Together with Kevin Burke, Torsvik has shown that reconstructed positions of Large Igneous Provinces (LIPs) that erupted in at least the past 200 Ma mostly coincide with present-day LLSVP margins. An explanation for this discovery is that LIPs are caused by plumes rising from the edges of LLSVPs, which implies relative stability of the LLSVP edges during this period. Such stability would be challenging to explain if the LLSVPs were purely thermal anomalies.

Regardless of their composition, the close proximity of LLSVPs to the core over potentially long timescales should elevate their temperatures. The surrounding mantle may therefore become hotter, less dense, and more buoyant (e.g. Figure 4c of Torsvik et al., 2016). Such negative density anomalies, at least above if not within the LLSVPs, have been invoked to explain the pattern of overlying geoid highs (Hager and Richards, 1989). In particular, if lower mantle viscosity is at least an order of magnitude higher than in the upper mantle, the negative geoid contribution of mass deficiencies at depth is outweighed by the positive geoid contribution associated with the upward deflection of the Earth's surface and core-mantle boundary by the generated upwelling (Richards and Hager, 1984) (that is, the degree two geoid sensitivity kernels become negative in the lower mantle (Hager et al., 1985)). An important consequence of this explanation is that LLSVPs should be overlain by positive dynamic topography on the order of 1 km in amplitude. Indeed, most geodynamic models of global mantle flow produce patterns of dynamic topography with long-wavelength amplitudes of about 1-km or more (see Flament et al. (2013) for a review of such models).

Is there independent evidence for such large amplitude dynamic topography at degree two? As far as we know, the present answer is no, although some studies have noted elevated long-wavelength topography in both the Pacific (McNutt, 1998) and Africa (Lithgow-Bertelloni and Silver, 1998). However, when one carefully corrects global topography for isostatic compensation of crust and cooling lithosphere, the resulting residual topography has a significantly smaller degree-two component compared to predictions from mantle flow models (Steinberger, 2016; Hoggard et al., 2016). Here we quantify this discrepancy in order to address this apparent paradox. We subsequently show that the lower mantle contribution to dynamic topography can only be dominant at spherical harmonic degree-two. Therefore, topographic discrepancies relating to the lower mantle are probably limited to degree-two. We will then consider the extent to which lateral viscosity variations (Čadek and Fleitout, 2003; Ghosh et al., 2010) in the upper mantle might be responsible for the over-predicting degree-two topography by geodynamic models (Flament et al., 2013; Conrad and Husson, 2009; Spasojevic and Gurnis, 2012). Finally, we discuss potential problems associated with other assumptions made by predictive models, and how they may be rectified to resolve the degree-two discrepancy.

2. Methodology

We compare an observation-based model of dynamic topography (global topography minus a model for isostatic topography) with a predictive model derived from a global mantle flow calculation. We note that many earlier predictive models of dynamic topography did not consider the contribution of density anomalies in the uppermost 220–350 km of the mantle (Flament et al., 2013). Topography at short wavelengths (high spherical harmonic degrees) is mainly generated by features that are close to the surface and therefore nearly fully isostatically compensated. In our model, we have chosen to include all velocity variations up to the surface, except within the continental lithosphere shallower than 150 km. Our definition of dynamic topography is therefore slightly different compared with previous studies. This difference is appropriate as long as predicted dynamic topography and observation-based residual topography are derived in a mutually consistent manner.

For our observation-based model of dynamic topography, we have combined the residual topography shown in Hoggard et al. (2016) for ocean regions with residual topography based on the crustal thickness and density model CRUST1.0 (Laske et al., 2013)for continental regions, where the residual topography model is hence very similar to Steinberger (2016). We have chosen this combination in order to sidestep the controversy surrounding the use of constant admittance to infer continental constraints directly from gravity anomalies (e.g. Molnar et al., 2015; Colli et al., 2016; Yang and Gurnis, 2016). Both models are global, but in the oceans, Hoggard's model is more advanced, as marine constraints are derived from a joint analysis of $\sim 2,000$ local, active source seismic experiments constraining sedimentary and crustal thickness, along with a global database of ship-track bathymetry (Hoggard et al., 2017). We have expanded Hoggard et al. (2016)'s residual topography to spherical harmonic degree 30 and divided by a factor 1.45 in order to convert from water coverage to "beneath air". For the CRUST1.0 model (Laske et al., 2013), residual topography is computed with the same correction for ocean floor subsidence with age and conversion to "beneath air" as for Hoggard et al. (2016), a nominal age of 175 Ma for continental regions, and expanded to degree 31. The nominal age for continents determines the relative elevation of oceans and continents after the correction and does not imply that we assume all continental lithosphere is as thick as 175-Ma old oceanic lithosphere; it is chosen so as to avoid sharp jumps at the transition from old ocean basins into continents. The global mean value of both the Hoggard et al. (2016) and the CRUST1.0-based residual topography models is then individually calculated and subtracted from these models, prior to their combination. The combined model is expanded in spherical harmonics up to degree 63, and subsequently re-evaluated on a grid considering degrees up to 31. Comparison of the topography pattern before and after combining the two separate spherical harmonic expansions into one shows that the main result is to smooth out the continent-ocean transition. The resulting residual topography map is shown in Figure 1a.

The predictive model of dynamic topography is driven by mantle density heterogeneity inferred from seismic tomography and follows Steinberger (2016) in the case without lateral viscosity variations. Seismic anomalies are directly scaled into temperature and density anomalies, except within continental lithosphere above 150 km depth and within the LLSVPs. This thermal conversion follows Steinberger and Calderwood (2006) where it has been derived from a compilation of mineral physics data. The conversion factor from relative anomalies of seismic shear-wave velocity v_s to relative anomalies of density ρ stays close to $\partial v_s/\partial\rho$ =0.25 throughout most of the mantle, similar to results obtained by others (e.g. Karato, 1993). In reality, the relation between seismic wavespeed and density is probably non-linear (Cammarano et al., 2003). For simplicity, we have not considered these effects here. The predictive model yields a radial stress at the surface that is converted to topography assuming air coverage, consistent with the residual topography model.

Our density model is derived from the SL2013sv seismic tomography of Schaeffer and Lebedev (2013) above 200 km depth and a 2010 update of Grand (2002) below. The upper mantle-only, isotropic model SL2013sv has comparatively high resolution due to inclusion of $\sim 750,000$ seismograms and the use of fundamental and higher mode surface waves alongside body waves. Its sub-plate seismic velocity variations have been shown to correlate well with residual topography constraints (e.g. Richards et al., 2016; Hoggard et al., 2017). We combine it with the update of Grand (2002) below 200 km depth, because we require a density model for the entire mantle, and this combination has been shown to yield a good fit with residual topography (Steinberger, 2016). We use the shallow tomographic constraints to produce lithospheric thickness maps. Essentially, seismic velocity variations are first converted to temperature variations and subsequently to absolute temperatures, assuming that the reference (zero-anomaly) seismic profile corresponds to a globally averaged thermal and compositional boundary layer. The base of the lithosphere is then assigned to a given constant temperature. Details of the procedure are described in Steinberger (2016). We assign a constant density to continental lithosphere shallower than 150 km, tuned in order to minimise the r.m.s. misfit between predicted and observed residual topography. This approach is a simple implementation of the isopycnal hypothesis of Jordan (1988), which states that strong seismic velocity variations in the lithosphere correspond to nearly zero density anomalies. Applying a direct thermal conversion to the entire continental lithosphere would cause strongly negative dynamic topography due to the omission of depletion buoyancy within continental lithosphere, which is inconsistent with observations. A large body of literature has since discussed the relations between density, seismic velocity and composition within the continental lithosphere. However, since this study is focused on contributions from the lower mantle, which – as we will show — likely dominate the degree-2 component, it will not be discussed further here.

We adjust the tomography-based predictive model in several ways to allow for better comparisons to the residual topography. We remove the dominant effect of ocean floor subsidence with age using Equation (5) from Hoggard et al. (2016), which is based upon the age-depth trend of Crosby and McKenzie (2009). Sharp jumps across the ocean-continent boundary are smoothed by assigning a nominal age value of 175 Ma to continental regions. These are the same corrections used in calculation of the observed residual topography model. Finally, for the case where LLSVPs are considered denser than the surrounding mantle, excess density of +1.2% has been added wherever the shear-wave anomaly drops below -1% in the lowermost 300 km of the mantle.

We test one prediction using purely radial viscosity variations along with a second version that allows for lateral viscosity variations (LVV) above 300 km. These lateral variations of effective viscosity occur because of temperature dependence, non-linear rheology and a reduced yield stress along plate boundaries. The method and model parameters are fully described in Osei Tutu et al. (2017). Essentially, we use a coupled code approach based on the instantaneous flow solutions computed with a modification of SLIM3D (Popov and Sobolev, 2008) above 300 km depth, and the spherical harmonics approach below that. That is, above 300 km the effective viscosity results from a combination of diffusion and dislocation creep, employing an Arrhenius temperature dependence law for both mechanisms. In the case of dislocation creep, we use a non-linear (power-law) relation between stress and strain rate, such that the effective viscosity also becomes strain rate dependent. We consider plastic yielding and yield stresses that are reduced along plate boundaries, such that the surface velocity field becomes approximately plate-like. See Popov and Sobolev (2008) for a more detailed description of this rheological approach. To achieve a coupling of the codes, tractions due to density anomalies below 300 km depth are computed with the spectral code and passed across the boundary at 300 km to the upper domain. Within the upper domain, flow velocities are then computed with SLIM3D and passed back across the coupling boundary as an upper boundary condition to the spectral mantle code. This procedure is iterated, until convergence has been achieved, i.e. the difference between two successive iterations has become sufficiently small. For more details, see Osei Tutu et al. (2017).

The viscosity structure in the case with only radial viscosity variations is adopted from Steinberger (2016) and similar to Steinberger and Calderwood (2006) where its derivation has been explained. Slight differences arise because Steinberger (2016) also considers the misfit between predicted and observed topography during the optimisation. The amplitude of computed dynamic topography is significantly larger than observed, but can be reduced by decreasing asthenospheric viscosity whilst increasing the lower mantle viscosity. Optimal root-mean-square fits to both geoid and topography (whereby a given weight is assigned to the individual fit) occur with an asthenospheric viscosity of $1.1 \cdot 10^{20}$ Pa s, about a factor 2.5 lower than in Steinberger and Calderwood (2006). Predicted amplitudes of dynamic topography can be further reduced to better match observations with even lower asthenospheric viscosity. However, this improvement comes at the expense of deteriorating fits to the geoid. Finally, in the scenario including LVV above 300 km (Osei Tutu et al., 2017; Osei Tutu et al.), we consider plastic yielding with friction coefficient 0.5 in plate interiors and yield stresses that are reduced along plate boundaries, with friction coefficient 0.03, such that the surface velocity field becomes approximately plate-like. We set a minimum viscosity cutoff 10^{18} Pa s within the asthenosphere and maximum viscosity of 10^{24} Pa s in the lithosphere. The viscosity model of Steinberger and Calderwood

Table 1: Correlations and amplitude ratios between dynamic and residual topography models

	corr		ratio	
	l=1-12	l=1-31	l=1-12	l=1-31
global, no LVV	0.61	0.57	1.18	1.22
oceans, no LVV	0.60	0.57	1.89	2.09
continents, no LVV	0.66	0.64	0.93	0.91
global, LVV	0.57	0.53	1.67	1.59
oceans, LVV	0.53	0.46	2.40	2.32
continents, LVV	0.61	0.58	1.45	1.37

(2006) is adopted below 300 km depth in this case.

3. Results

Figure 1b shows predicted dynamic topography for purely radial viscosity variations. Correlations and amplitude ratios between residual topography (Figure 1a) and dynamic topography (Figure 1b and c), globally or for oceans or continents alone, with or without LVV, are given in Table 1. Throughout the discussion, values for l = 1–31 will be followed by values for l = 1–12 in parentheses. Results are similar to what Steinberger (2016) found except that the correlation in the oceans has noticeably improved. However, the r.m.s. amplitude ratio in the oceans has now increased, due to the lower magnitudes of oceanic dynamic topography in the Hoggard et al. (2016) model. If we instead use the full observation-based model of Hoggard et al. (2016), global correlations reduce to 0.46 (0.48), dominated by poor fits to continental regions of only 0.34 (0.34). We will therefore proceed with our new, combined model of observed residual topography. Our results also stand up well to a visual comparison, with many similar oceanic and continental features present in panels 1a and 1b. However, oceanic variations have much lower amplitude in the observation model compared to the predictions. This discrepancy was also pointed out by Hoggard et al. (2016).

One possible explanation for this discrepancy could be the omission of lateral viscosity variations. For example, lower viscosity asthenosphere in the oceans may encourage lateral flow and divergence of upwellings, decoupling deep mantle flow from the lithosphere and reducing dynamic topography. Figure 1c shows predicted dynamic topography when LVV above 300 km depth have been included. The principal difference with Figure 1b is that amplitudes of continental dynamic topography are increased. This effect occurs because continental lithosphere ends up with a comparatively stronger rheology, which efficiently couples density anomalies in the upper mantle to the surface.

In order to partly compensate for this effect and re-calibrate the fit with residual topography, density depletion in the continental lithosphere above 150 km has been changed to -0.6%. However, r.m.s. topography amplitudes are still 37% (45%) too high in the continents following this correction, with correlation of 0.58 (0.61). In the oceans, r.m.s. amplitudes of topography are now a factor 2.32 (2.40) too large, with correlation of 0.46 (0.53). The global correlation is 0.53 (0.57), and the r.m.s. amplitude of the mantle-flow derived dynamic topography is 59% (67%) too high. We attribute these increased amplitudes to the fact

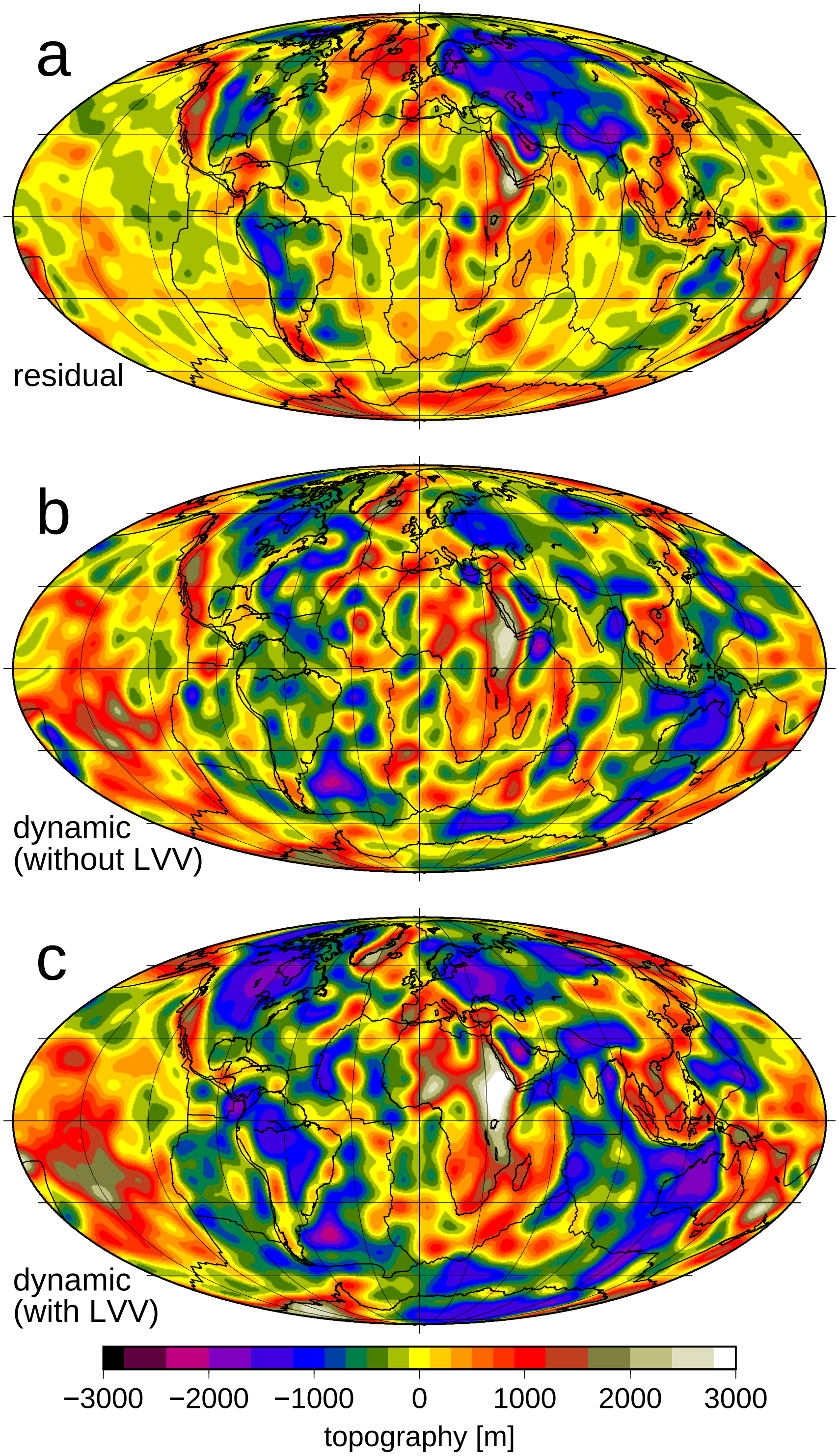

Figure 1: Maps of observation-based and predicted dynamic topography. (a) Computed residual topography based upon marine constraints from Hoggard et al. (2016) and continental constraints following Steinberger (2016). Minor deviations from the Steinberger (2016) reference model arise due to adoption of an alternative age-depth trend and use of a density change of $\delta\rho_l = -0.25\%$ for continental lithosphere shallower than 150 km. (b) Predicted dynamic topography using a purely radial viscosity profile with density anomalies generated from SL2013sv tomography model above 200 km and TX2011 below (Schaeffer and Lebedev, 2013; Grand, 2002). (c) Version that also includes the effect of lateral viscosity variations above 300 km (Osei Tutu et al., 2017). All maps are expanded to maximum spherical harmonic degree $l_{\max} = 31$. For dynamic topography computations, stresses are converted to topography "beneath air" and accordingly oceanic residual topography is divided by a factor 1.45 for consistency.

that a lithosphere with strong plate interiors and weak plate boundaries yields larger dynamic topography variations than appropriate constant lithospheric viscosity (as in the case without LVV). Steinberger (2016) found an $\sim 20\%$ increase for models with prescribed plate motions. In our model with LVV, the plates move freely in response to forces acting upon them. However, given the good match between our predicted plate velocities and those observed (Osei Tutu et al.), dynamic topography is similar with prescribed plate motions and with plates moving freely.

In the oceans, the effect of plate-like velocities amplifying predicted dynamic topography is partly compensated by the lower viscosity asthenosphere and poor coupling to deep mantle flow. The rheological model used by Osei Tutu et al. (2017) gives an effective viscosity of oceanic asthenosphere of $\sim 10^{19}$ Pa s, which is only moderately reduced compared to the reference case without LVV of $1.1 \cdot 10^{20}$ Pa s. The resulting reduction in dynamic topography is estimated to be only 6-7% (see Figure 9 of Steinberger, 2016). The interaction of these two opposing effects therefore slightly increases r.m.s. amplitudes of predicted dynamic topography, even in the oceanic realm.

We have shown that introducing LVV can make the r.m.s. amplitude excess more similar between oceanic and continental regions. However, LVV does not remove the degree-two discrepancy, and so we will continue with the purely radial model for simplicity. The amplitude spectra of observed residual topography and predicted dynamic topography are shown in Figure 2a. The largest mismatch occurs at degree-two where predictions have more than twice the amplitude of observations. Amplitude is also too high for $l \geq 6$, although this appears to be specific to our particular SL2013sv + TX2011 density model. We note that a density model based upon SAVANI (Auer et al., 2014) yields amplitude more closely matching observations for $l = 3$ to 5 and most degrees $l > 15$, with a similar match for most other degrees and similar correlation (Figure 2b), but fits the geoid less well (Steinberger, 2016). Similar amplitude but poorer correlation is observed for other tomography models (see Figure 10b in Steinberger, 2016).

The slope of $l > 2$ amplitude spectra for the predictive models shown in Figure 1 and Steinberger (2016) are similar to those of the observation-based model. These slopes are considerably shallower than the five predictive models shown in Figure 5b of Hoggard et al. (2016). This improvement is a direct consequence of including density anomalies right up to the surface and the improved resolution of modern, upper mantle tomography models. Our preferred SL2013sv + TX2011 reference prediction provides relatively high correlation with observed residual topography, whilst simultaneously matching observed geoid anomalies (Steinberger, 2016). However, in contrast to higher degrees, the amplitude discrepancy at $l = 2$ occurs for all tomography models tested by Steinberger (2016). This reflects the fact that long-wavelength mantle structure is more robustly imaged and therefore similar between models.

To further pin down the source of this discrepancy, the contributions of the upper and lower mantle on either side of 660 km are considered separately (Figure 3). The lower mantle signal is dominated by degree-two. Highs occur above the African and Pacific LLSVPs with lows in the Americas and in southeast Asia where most recent subduction is concentrated. In contrast, all smaller-scale dynamic topography is generated within the upper mantle.

This visual impression is confirmed when we look at spectral amplitude for the upper and lower mantle in isolation (Figure 4). The lower mantle dominates for degree-two whilst the upper mantle provides a larger

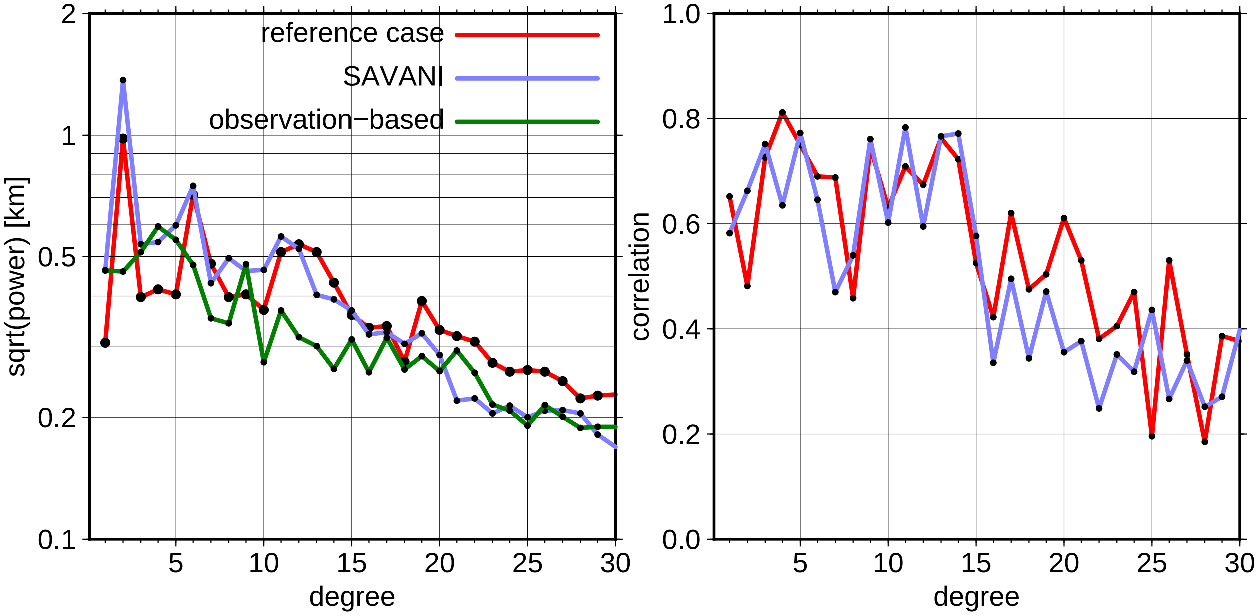

Figure 2: Spectral analysis of dynamic topography. (a) Amplitude (square root of power) spectra of our observation-based model and predictions calculated using purely radial viscosity variations and density models derived from either SL2013sv + TX2011 or SAVANI tomography. SAVANI prediction is similar to Steinberger (2016), but with $\delta\rho_l = -0.3\%$ continental lithospheric density reduction above 150 km. (b) Correlation between predicted dynamic topography and observed residual topography.

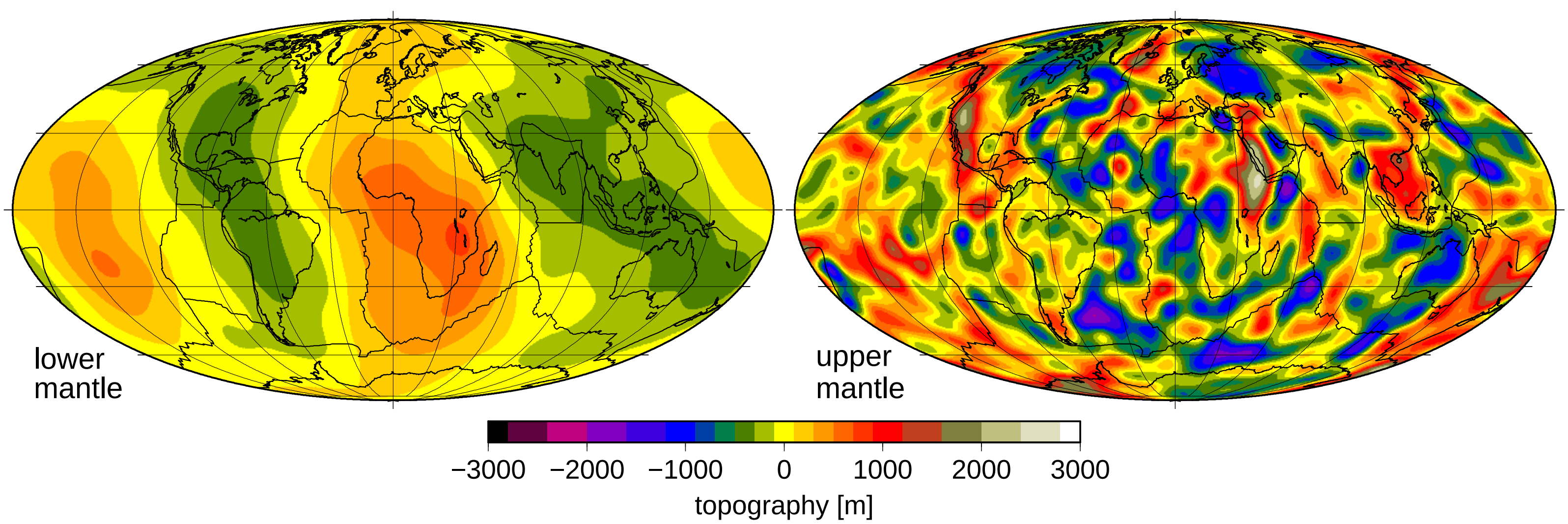

Figure 3: Contribution to predicted dynamic topography from (a) the lower mantle beneath 660 km and (b) the upper mantle for the SL2013sv + TX2011 model with no LVV (Figure 1b).

contribution for all other degrees. In particular, the upper mantle contribution exeeds that of the lower mantle by at least a factor 6 in amplitude for all $l \geq 6$. We therefore infer that there are likely to be different reasons causing the $l \geq 6$ discrepancy between predictions and observations versus those at $l = 2$. The former appears to be related to anomalies in the upper mantle, whilst the latter relates to contributions from the lower mantle.

In our preferred SL2013sv + TX2011 reference prediction, we already consider that LLSVPs may be compositionally distinct. However, our +1.2% density increase only results in an $\sim 2\%$ reduction in the amplitude of dynamic topography (Steinberger, 2016). At degree 2, the amplitude is reduced by 10 %. We can assume that the volume of these piles is potentially much larger, or even create an extreme scenario whereby all of the low-density mass deficiencies (inferred from slow shear-wave velocities) in the lower mantle are set to zero. However, the degree-two contribution is still over-predicted due to the effects of fast shear-wave velocities and excess mass related to slabs that surround LLSVP locations. In essence, Figure 4 illustrates that the correct amount of degree two amplitude can be obtained without any contribution from the lower mantle.

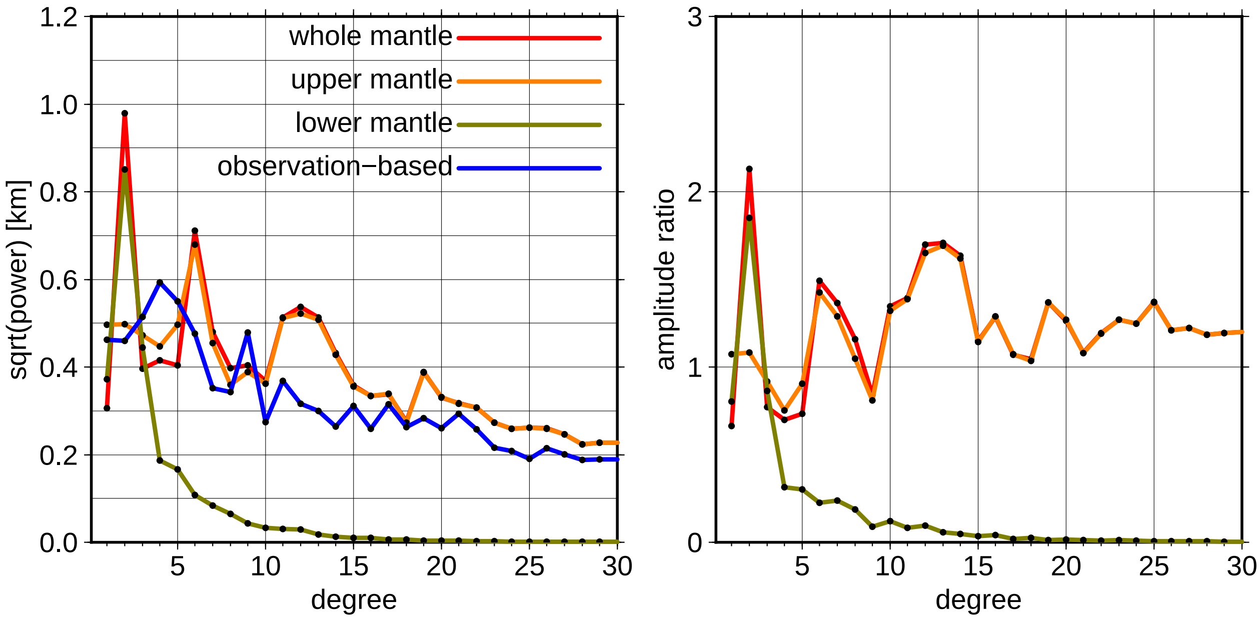

Figure 4: (a) Amplitude (square root of power) spectra as in Figure 2a, including the separate contributions of upper and lower mantle shown in Figure 3. (b) Amplitude ratio for each component relative to the observation-based residual topography model.

4. Discussion

The amplitude of dynamic topography supported by mantle flow driven by tomographically-constrained density heterogeneity is greater than the amplitude of residual topography inferred from observation. This descripancy is dominated by overly-large dynamic topography predicted for degree-2, which is more than twice the amplitude inferred from residual topography and arises from flow driven by lower mantle density heterogeneity. Our preferred predictive flow model, which uses densities derived from the SL2013sv and TX2011 tomography models (Schaeffer and Lebedev, 2013; Grand, 2002), also overpredicts dynamic topography amplitudes for degrees $l \geq 6$ (wavelengths shorter than $\sim 7,300$ km), which arise from upper mantle flow, but only by about 40% and with an amplitude spectra slope that approximately matches that for residual topography (Figure 2 a). This similar slope is achieved because density anomalies are considered up to the surface. If they were removed in the uppermost mantle, the slope for the predicted dynamic topography would be steeper (see e.g. Figure 5 b in Hoggard et al., 2016). Other tomography models (Figure 2 a, see also Figure 10 b of Steinberger (2016)) yield lower amplitudes for degrees $l \geq 15$, but exhibit poorer correlations to observed residual topography or geoid anomalies. However, an over-prediction of amplitude for degrees 6 to 14, with the notable exception of degree 9, appears to be a more general outcome for different tomography models. The resolution of seismic tomography models has steadily increased as larger datasets and more intensive computational techniques have become available. Further improvements might lead to an upper mantle density model that yields improved fit for $l \geq 6$ dynamic topography in terms of both pattern and amplitude. However, given that degree-two structure has been consistently imaged for many years, it remains unlikely that the degree-two mismatch will be resolved purely using newer generations of tomography models.

Which other factors could cause this degree-two discrepancy? Perhaps the simplest answer would be that observation-based estimates of residual topography are too low. This option has been suspected by Yang and Gurnis (2016) and partly attributed to Hoggard et al. (2016) using free-air gravity anomalies to infer dynamic topography in continental regions. Indeed, the use of a constant admittance value is an area of ongoing debate (e.g. Molnar et al., 2015; Colli et al., 2016). In order to address this issue, we combined the Hoggard et al. (2016) model from the oceans, where it is free from gravity-derived constraints, with continental estimates calculated using CRUST1.0. We find that this omission of gravity data still results in a large mismatch at degree-two. A similar discrepancy also occurs for a model derived purely from CRUST1.0 (see Figure 10 b in Steinberger, 2016). In fact, the two separate residual topography models have a high correlation of 0.71 (0.78) in the oceans, but the Hoggard et al. (2016) model has a 20% (23%) lower amplitude. Also, visual comparison of models reviewed by Flament et al. (2013) shows a degree-two signal clearly visible in dynamic topography predictions, while it can be hardly seen for the residual topography models reviewed by that study. Hence, the discrepancy has been aggravated in the Hoggard et al. (2016) model, but also occurs in less sophisticated models for residual topography.

If the observation-based estimates of small-amplitude degree-2 dynamic topography remain robust, then we must alternatively look for explanations for why the amplitudes of dynamic topography predicted by global flow models remain too large. For example, we have tested the effects of lateral viscosity variations in the upper mantle. However, we find that the general characteristics of predicted dynamic topography remain similar to the radially-varying viscosity case, and the fit to observed residual topography and geoid variations is not improved. Some improvement of fit for LVV might be achieved by fine-tuning some of the rheological properties, but has not been attempted here. Given the preliminary results in this study, we do not expect such an effort to result in substantial improvements to the degree-two discrepancy.

Strong lateral variations in rheology deeper than 300 km may also influence the pattern of dynamic topography. For example, the recent BEAMS hypothesis of Ballmer et al. (2017) states that there are strong silica-enriched domains in the Earth's lower mantle that essentially do not participate in whole-mantle convection. Sinking slabs and rising plumes are focused into narrow regions between the BEAMS, thus altering the planform of convection. An alternative mechanism that may limit upwellings and downwellings to narrow zones is anisotropic viscosity (Wheeler, 2010). Regions with large density anomalies and associated stresses can concentrate deformation. Shear along these zones can cause alignment of the fabric and planes of weakness that are subsequently re-exploited, thereby localising convective flow. Both of these mechanisms may substantially alter the pattern of mantle convection. However, direct consequences for degree-two dynamic topography are harder to estimate because they depend upon the spatial location of concentrated flow. Degree-two amplitudes may even be enhanced if slabs preferentially sink along the Pacific Ring of Fire, or plumes preferentially cluster over LLSVPs.

An alternative explanation might be to alter the radial viscosity profile of the mantle in order to reduce degree-two dynamic topography. Viscosity variations within the mantle remain poorly constrained and a wide range of possibilities have been published, even within the last couple of years (e.g. Justo et al., 2015; Marquardt and Miyagi, 2015; Rudolph et al., 2015; King, 2016; Lau et al., 2016; Liu and Zhong, 2016). Importantly, altering the viscosity structure too severely is likely to erode the quality of fit to geoid anomalies. Dynamic topography at the surface is a significant contribution to the geoid. It therefore remains to be seen whether altering the radial viscosity profile can substantially reduce the degree-two discrepancy whilst simultaneously preserving a good geoid fit.

An obvious way to alter the discrepancy would be to reduce the scaling from seismic velocity to density anomalies in the lower mantle. For example, additional positive density could also be assigned to seismically slow and presumably hot regions of the mantle to simulate the possible effects of chemical heterogeneity. As has been pointed out by Guerri et al. (2016), considering chemical heterogeneities in correspondence with the lower mantle LLSVPs helps to decrease the peak-to-peak amplitudes of dynamic topography and geoid, but significantly reduces the correlation between synthetic and observed geoid. However, a significant reduction of density heterogeneity throughout the lower mantle would be required to decrease the predicted degree-two dynamic topography sufficiently. This is because the amplitude of degree-two dynamic topography is rather insensitive to density heterogeneity near the LLSVPs (the dynamic topography kernel is close to zero in the lowermost mantle). Furthermore, the required reduction in dynamic topography amplitude by more than a factor of 2 (Fig. 4a) means that even the assignment of zero density anomaly to all low-velocity anomalies in the lower mantle would still produce dynamic topography degree-two amplitudes that are too large; the over-prediction would be reduced by about half, but in order to completely remove it, it would also be necessary to reduce the amplitude for the high-density anomalies (fast seismic velocities that are inferred to be slabs). This is problematic because tectonic histories suggest a long history of subduction that has been linked to seismic tomography (e.g., van der Meer et al., 2012) and the lower mantle density heterogeneity of slabs has been linked to other observables such as seismic anisotropy (Becker et al., 2014) and plate-driving forces (e.g., Lithgow-Bertelloni and Silver, 1998; Becker and O'Connell, 2001; van Summeren et al., 2012). Furthermore, Conrad et al. (2013) have shown that computed flow closely matches general patterns of global plate motion, particularly for the dipole and quadrupole components (spherical harmonic degrees 1 and 2). Indeed, it is important to remember that existing mantle convection models driven by both postive and negative density heterogeneities throughout the mantle have been very successful in explaining a variety of observations such as plate motions, lithosphere stresses and seismic anisotropy, and their successful prediction of geoid anomalies may be particularly difficult to reconcile with signficant changes to the amplitude of long-wavelenth dynamic topography. These simple relationships must be maintained when introducing additional modifications and complexities.

5. Conclusions

Mantle convection models predict dynamic topography that has larger amplitudes than inferred from observations. At spherical harmonic degree two, predicted topography is largely generated by density anomalies in the lower mantle. Anomalies in the upper mantle yield similar amplitude at degree three and are the clearly dominant contribution at all other degrees. We show that the discrepancy between observed and predicted topography is largest at degree two, occurs for a wide range of seismic tomography models and is consistent between different models of observed residual topography.

This discrepancy could possibly be resolved if the scaling factor from seismic to density anomalies is much lower than is generally assumed by mantle flow models. Alternatively, mantle flow may be largely restricted to smaller-scale features such as rising plumes and sinking slabs, with very little large-scale flow in between. Mechanisms that may give rise to such patterns are gernally associated with highly heterogeneous or anisotropic lower mantle viscosity. However, when invoking such a scenario, it is important to consider that current mantle flow models dominated by large-scale flow can successfully explain most of the geoid and current plate motions. Revised models of mantle flow must also be capable of reproducing these fundamental observations.

Acknowledgements

BS thanks all the people coming to the poster at EGU 2017 for discussions. This work was partially funded by the Research Council of Norway Centre of Excellence Project 223272. We thank the editor Philippe Agard and two anonymous reviewers for their valuable comments.

References

Auer, L., Boschi, L., Becker, T.W., Nissen-Meyer, T., Giardini, D., 2014. Savani: A variable-resolution whole-mantle model of anisotropic shear-velocity variations based on multiple datasets. J. Geophys. Res. 119, 3006–3034. doi:10.1002/2013JB010773.

Austermann, J., Kaye, B.T., Mitrovica, J.X., Huybers, P., 2014. A statistical analysis of the correlation between large igneous provinces and lower mantle seismic structure. Geophys. J. Int. 197, 1–9. doi:10.1093/gji/ggt500.

Ballmer, M.D., Houser, C., Hernlund, J.W., Wentzcovitch, R.M., Hirose, K., 2017. Persistence of strong silica-enriched domains in the Earths lower mantle. Nat. Geosci. 10, 236–240. doi:10.1038/ngeo2898.

Ballmer, M.D., Schumacher, L., Lekic, V., Thomas, C., Ito, G., 2016. Compositional layering within the large low shear-wave velocity provinces in the lower mantle. Geochem., Geophys., Geosys. 17, 5056–5077. doi:10.1002/2016GC006605.

Becker, T.W., Conrad, C.P., Schaeffer, A.J., Lebedev, S., 2014. Origin of azimuthal seismic anisotropy in oceanic plates and mantle. Earth Planet. Sci. Lett. 401, 236–250. doi:10.1016/j.epsl.2014.06.014.

Becker, T.W., O'Connell, R.J., 2001. Predicting plate velocities with mantle circulation models. Geochem., Geophys., Geosys. 2, 1060. doi:10.1029/2001GC000171.

Bull, A.L., Domeier, M., Torsvik, T.H., 2014. The effect of plate motion history on the longevity of deep mantle heterogeneities. Earth Planet. Sci. Lett. 401, 172–182. doi:10.1016/j.epsl.2014.06.008.

Čadek, O., Fleitout, L., 2003. Effect of lateral viscosity variations in the top 300 km of the mantle on the geoid and dynamic topography. Geophys. J. Int. 152, 566–580. doi:10.1046/j.1365-246X.2003.01859.x.

Cammarano, F., Goes, S., Vacher, P., Giardini, D., 2003. Inferring upper-mantle temperatures from seismic velocities. Phys. Earth Planet. Inter. 138, 197–222. doi:10.1016/S0031-9201(03)00156-0.

Colli, L., Ghelichkhan, S., Bunge, H.P., 2016. On the ratio of dynamic topography and gravity anomalies in a dynamic Earth. Geophys. Res. Lett. 43, 1–7. doi:10.1002/2016GL067929.

Conrad, C.P., Husson, L., 2009. Influence of dynamic topography on sea level and its rate of change. Lithosphere 1, 110–120. doi:10.1130/L32.1.

Conrad, C.P., Steinberger, B., Torsvik, T.H., 2013. Stability of active mantle upwelling revealed by net characteristics of plate tectonics. Nature 498, 479–482. doi:10.1038/nature12203.

Courtillot, V., Davaille, A., Besse, J., Stock, J., 2003. Three distinct types of hotspots in the Earth's mantle. Earth Planet. Sci. Lett. 205, 295–308. doi:10.1016/S0012-821X(02)01048-8.

Crosby, A.G., McKenzie, D.P., 2009. An analysis of young ocean depth, gravity and global residual topography. Geophys. J. Int. 178, 1198–1219. doi:10.1111/j.1365-246X.2009.04224.x.

Davies, D.R., Goes, S., Davies, J.H., Schuberth, B.S.A., Bunge, H.P., Ritsema, J., 2012. Reconciling dynamic and seismic models of Earth's lower mantle: The dominant role of thermal heterogeneity. Earth Planet. Sci. Lett. 353-354, 253–269. doi:10.1016/j.epsl.2012.08.016.

Davies, D.R., Goes, S., Sambridge, M., 2015. On the relationship between volcanic hotspot locations, the reconstructed eruption sites of large igneous provinces and deep mantle seismic structure. Earth Planet. Sci. Lett. 411, 121–130. doi:10.1016/j.epsl.2014.11.052.

Doubrovine, P.V., Steinberger, B., Torsvik, T.H., 2016. A failure to reject: Testing the correlation between large igneous provinces and deep mantle structures with EDF statistics. Geochem., Geophys., Geosys. 17, 1130–1163. doi:10.1002/2015GC006044.

Dziewonski, A.M., Hager, B.H., O'Connell, R.J., 1977. Large-scale heterogeneities in the lower mantle. J. Geophys. Res. 82, 239–255. doi:10.1029/JB082i002p00239.

Dziewonski, A.M., Lekic, V., Romanowicz, B.A., 2010. Mantle anchor structure: An argument for bottom up tectonics. Earth Planet. Sci. Lett. 299, 69–79. doi:10.1016/j.epsl.2010.08.013.

Flament, N., Gurnis, M., D., M.R., 2013. A review of observations and models of dynamic topography. Lithosphere 5, 189–210. doi:10.1130/l245.1.

Frost, D.A., Rost, S., 2014. The P-wave boundary of the Large-Low Shear Velocity Province beneath the Pacific. Earth Planet. Sci. Lett. 403, 380–392. doi:10.1016/j.epsl.2014.06.046.

Garnero, E.J., McNamara, A.K., Shim, S.H., 2016. Continent-sized anomalous zones with low seismic velocity at the base of Earth's mantle. Nat. Geosci. 9, 481–489. doi:10.1038/ngeo2733.

Ghosh, A., Becker, T., Zhong, S.J., 2010. Effects of lateral viscosity variations on the geoid. Geophys. Res. Lett. 37, L01301. doi:10.1029/2009GL040426.

Grand, S.P., 2002. Mantle shear-wave tomography and the fate of subducted slabs. Phil. Trans. R. Soc. Lond. A 360, 2475–2491. doi:10.1098/rsta.2002.1077.

Guerri, M., Cammarano, F., Tackley, P.J., 2016. Modelling Earth's surface topography: Decomposition of the static and dynamic components. Phys. Earth Planet. Inter. 261, 172–186. doi:10.1016/j.pepi.2016.10.009.

Hager, B.H., Clayton, R.W., Richards, M.A., 1985. Lower mantle heterogeneity, dynamic topography and the geoid. Nature 313, 541–545. doi:10.1038/313541a0.

Hager, B.H., Richards, M.A., 1989. Long-wavelength variations in Earth's geoid: physical models and dynamical implications. Phil. Trans. R. Soc. London Ser. A 328, 309–327. doi:10.1098/rsta.1989.0038.

Hoggard, M.J., White, N., Al-Attar, D., 2016. Global dynamic topography observations reveal limited influence of large-scale mantle flow. Nat. Geosci. 9, 456–463. doi:10.1038/ngeo2709.

Hoggard, M.J., Winterbourne, J., Czarnota, K., White, N., 2017. Oceanic residual depth measurements, the plate cooling model, and global dynamic topography. J. Geophys. Res. Solid Earth 122, 2328–2372. doi:10.1002/2016JB013457.

Ishii, M., Tromp, J., 2004. Constraining large-scale mantle heterogeneity using mantle and inner-core sensitive normal modes. Phys. Earth Planet. Inter. 146, 113–124. doi:10.1016/j.pepi.2003.06.012.

Jordan, T.H., 1988. Structure and formation of the continental tectonosphere. J. Petrol. Special Volume (1), 11–37. doi:10.1093/petrology/Special_Volume.1.11.

Justo, J.F., Morra, G., Yuen, D.A., 2015. Viscosity undulations in the lower mantle: The dynamical role of iron spin transition. Earth Planet. Sci. Lett. 421, 20–26. doi:10.1016/j.epsl.2015.03.013.

Karato, S.i., 1993. Importance of anelasticity in the interpretation of seismic tomography. Geophys. Res. Lett. 20, 1623–1626. doi:10.1029/93GL01767.

King, S.D., 2016. An evolving view of transition zone and midmantle viscosity. Geochem., Geophys., Geosys. 17, 1234–1237. doi:10.1002/2016GC006279.

Koelemeijer, P., Deuss, A., Ritsema, J., 2017. Density structure of Earth's lowermost mantle from Stoneley mode splitting observations. Nat. Commun. 8, 15241. doi:10.1038/ncomms15241.

Laske, G., Masters., G., Ma, Z., Pasyanos, M., 2013. Update on CRUST1.0 - a 1-degree global model of Earth's crust. Geophys. Res. Abstr. 15. Abstract EGU2013-2658.

Lassak, T.M., McNamara, A.K., Garnero, E.J., Zhong, S.J., 2010. Core-mantle boundary topography as a possible constraint on lower mantle chemistry and dynamics. Earth Planet. Sci. Lett. 289, 232–241. doi:10.1016/j.epsl.2009.11.012.

Lau, H.C.P., Mitrovica, J.X., Austermann, J., Crawford, O., Al-Attar, D., Latychev, K., 2016. Inferences of mantle viscosity based on ice age data sets: Radial structure. J. Geophys. Res. Solid Earth 121, 6991–7012. doi:10.1002/2016JB013043.

Lau, H.C.P., Mitrovica, J.X., Davis, J.L., Tromp, J., Yang, H.Y., Al-Attar, D., 2017. Tidal tomography constrains Earths deep-mantle buoyancy. Nature 551, 321–326. doi:10.1038/nature24452.

Lekic, V., Cottaar, S., Dziewonski, A., Romanowicz, B., 2012. Cluster analysis of global lower mantle tomography: A new class of structure and implications for chemical heterogeneity. Earth Planet. Sci. Lett. 357–358, 68–77. doi:10.1016/j.epsl.2012.09.014.

Lithgow-Bertelloni, C., Silver, P.G., 1998. Dynamic topography, plate driving forces and the African superswell. Nature 395, 269–272. doi:10.1038/26212.

Liu, X., Zhong, S., 2016. Constraining mantle viscosity structure for a thermochemical mantle using the geoid observation. Geochem., Geophys., Geosys. 17, 895–913. doi:10.1002/2015GC006161.

Marquardt, H., Miyagi, L., 2015. Slab stagnation in the shallow lower mantle linked to an increase in mantle viscosity. Nat. Geosci. 8, 311–314. doi:10.1038/ngeo2393.

Masters, G., Laske, G., Bolton, H., Dziewonski, A., 2000. The relative behavior of shear velocity, bulk sound speed, and compressional velocity in the mantle: implications for chemical and thermal structure, in: Karato, S., Forte, A., Liebermann, R., Masters, G., Stixrude, L. (Eds.), Seismology and Mineral Physics. American Geophysical Union, Washington DC. volume 117 of *AGU Gepophys. Mono.*, pp. 63–87.

McNutt, M.K., 1998. Superswells. Rev. Geophys. 36, 211–244. doi:10.1029/98RG00255.

van der Meer, D.G., Torsvik, T.H., Spakman, W., van Hinsbergen, D.J.J., Amaru, M.L., 2012. Intra-Panthalassa Ocean subduction zones revealed by fossil arcs and mantle structure. Nat. Geosci. 5, 215–219. doi:10.1038/ngeo1401.

Molnar, P., England, P.C., Jones, C.H., 2015. Mantle dynamics, isostasy, and the support of high terrain. J. Geophys. Res. 120, 1932–1957. doi:10.1002/2014JB011724.

Ni, S., Tan, E., Gurnis, M., Helmberger, D., 2002. Sharp sides to the African superplume. Science 296, 1850–1852. doi:10.1126/science.1070698.

Osei Tutu, A., Steinberger, B., Sobolev, S.V., Popov, A., Rogozhina, I., . Evaluating the influence of plate boundary friction and mantle viscosity on plate velocities. Geochem., Geophys., Geosys. , in review.

Osei Tutu, A., Steinberger, B., Sobolev, S.V., Popov, A., Rogozhina, I., 2017. Effects of upper mantle heterogeneities on lithospheric stress field and dynamic topography. Solid Earth Discuss , in review.doi:10.5194/se-2017-111.

Popov, A.A., Sobolev, S.V., 2008. SLIM3D: A tool for three-dimensional thermomechanical modeling of lithospheric deformation with elasto-visco-plastic rheology. Phys. Earth Planet. Inter. 171, 55–75. doi:10.1016/j.pepi.2008.03.007.

Richards, F.D., Hoggard, M.J., White, N.J., 2016. Cenozoic epeirogeny of the Indian peninsula. Geochem., Geophys., Geosys. 17, 4920–4954. doi:10.1002/2016GC006545.

Richards, M.A., Hager, B.H., 1984. Geoid anomalies in a dynamic Earth. J. Geophys. Res. 89, 5987–6002. doi:10.1029/JB089iB07p05987.

Rudolph, M.L., Lekić, V., Lithgow-Bertelloni, C., 2015. Viscosity jump in Earths mid-mantle. Science 350, 1349–1352. doi:10.1126/science.aad1929.

Schaeffer, A., Lebedev, S., 2013. Global shear speed structure of the upper mantle and transition zone. Geophys. J. Int. 194, 417–449. doi:10.1093/gji/ggt095.

Schuberth, B.S.A., Zaroli, C., Nolet, G., 2012. Synthetic seismograms for a synthetic Earth: long-period P- and S-wave traveltime variations can be explained by temperature alone. Geophys. J. Int. 188, 1393–1412. doi:10.1111/j.1365-246X.2011.05333.x.

Spasojevic, S., Gurnis, M., 2012. Sea level and vertical motion of continents from dynamic earth models since the Late Cretaceous. Am Assoc. Petr. Geol. B. 96, 2037–2064. doi:10.1306/03261211121.

Steinberger, B., 2016. Topography caused by mantle density variations: observation-based estimates and models derived from tomography and lithosphere thickness. Geophys. J. Int. 205, 604–621. doi:10.1093/gji/ggw040.

Steinberger, B., Calderwood, A., 2006. Models of large-scale viscous flow in the Earth's mantle with constraints from mineral physics and surface observations. Geophys. J. Int. 167, 1461–1481. doi:10.1111/j.1365-246X.2006.03131.x.

Steinberger, B., Torsvik, T., 2012. A geodynamic model of plumes from the margins of Large Low Shear Velocity Provinces. Geochem., Geophys., Geosys. 13, Q01W09. doi:10.1029/2011GC003808.

Su, W., Dziewonski, A.M., 1991. Predominance of long-wavelength heterogeneity in the mantle. Nature 352, 121–126. doi:10.1038/352121a0.

Su, W.j., Dziewonski, A.M., 1997. Simultaneous inversion for 3-D variations in shear and bulk velocity in the mantle. Phys. Earth Planet. Inter. 100, 135–156. doi:10.1016/S0031-9201(96)03236-0.

van Summeren, J., Conrad, C.P., Lithgow-Bertelloni, C., 2012. The importance of slab pull and a global asthenosphere to plate motions. Geochem., Geophys., Geosys. 13, Q0AK03. doi:10.1029/2011gc003873.

Thorne, M.S., Garnero, E.J., Grand, S.P., 2004. Geographic correlation between hot spots and deep mantle lateral shear-wave velocity gradients. Phys. Earth Planet. Inter. 146, 47–63. doi:10.1016/j.pepi.2003.09.026.

To, A., Romanowicz, B., Capdeville, Y., T., N., 2005. 3D effects of sharp boundaries at the borders of the African and Pacific Superplumes: Observation and modeling. Earth Planet. Sci. Lett. 233, 137–153. doi:10.1016/j.epsl.2005.01.037.

Torsvik, T.H., Smethurst, M.A., Burke, K., Steinberger, B., 2006. Large igneous provinces generated from the margins of the large low-velocity provinces in the deep mantle. Geophys. J. Int. 167, 1447–1460. doi:10.1111/j.1365-246X.2006.03158.x.

Torsvik, T.H., Steinberger, B., Ashwal, L.D., Doubrovine, P.V., Trønnes, R.G., 2016. Earth evolution and dynamics – a tribute to Kevin Burke. Can. J. Earth Sci. 53, 1073–1087. doi:10.1139/cjes-2015-0228.

Wang, Y., Wen, L., 2004. Mapping the geometry and geographic distribution of a very low velocity province at the base of the Earth's mantle. J. Geophys. Res. 109. doi:10.1029/2003JB002674.

Wheeler, J., 2010. Anisotropic rheology during grain boundary diffusion creep and its relation to grain rotation, grain boundary sliding and superplasticity. Philos. Mag. 90, 2841–2864. doi:10.1080/14786431003636097.

Yang, T., Gurnis, M., 2016. Dynamic topography, gravity and the role of lateral viscosity variations from inversion of global mantle flow. Geophys. J. Int. 207, 1186–1202. doi:10.1093/gji/ggw335.